

Uncertainties in modeling low-energy neutrino induced reactions on iron group nuclei

N. Paar¹, T. Suzuki², M. Honma³, T. Marketin^{1,4}, D. Vretenar¹

¹*Physics Department, Faculty of Science, University of Zagreb, Croatia*

²*Department of Physics, College of Humanities and Sciences, Nihon University, Sakurajosui 3-25-40, Setagaya-ku, Tokyo 156-8550, Japan*

³*Center for Mathematical Sciences, University of Aizu, Aizu-Wakamatsu, Fukushima 965-8580, Japan and*

⁴*GSI Helmholtzzentrum für Schwerionenforschung, Planckstraße 1, D-64291 Darmstadt, Germany*

Charged-current neutrino-nucleus cross sections for ^{54,56}Fe and ^{58,60}Ni are calculated and compared using frameworks based on relativistic and Skyrme energy density functionals, and the shell model. The current theoretical uncertainties in modeling neutrino-nucleus cross sections are assessed in relation to the predicted Gamow-Teller transition strength and available data, multipole decomposition of the cross sections, and cross sections averaged over the Michel flux and Fermi-Dirac distribution. Employing different microscopic approaches and models, the DAR neutrino-⁵⁶Fe cross section and its theoretical uncertainty are estimated: $\langle \sigma \rangle_{th} = (258 \pm 57) \times 10^{-42} \text{cm}^2$, in very good agreement with the experimental value: $\langle \sigma \rangle_{exp} = (256 \pm 108 \pm 43) \times 10^{-42} \text{cm}^2$.

PACS numbers: 21.30.Fe, 21.60.Jz, 23.40.Bw, 25.30.-c

Weak neutrino-induced processes in nuclei provide information of relevance for modeling the response in neutrino detectors, understanding the fundamental properties of the weak interaction, and the role of neutrinos in stellar environment. Data on neutrino-nucleus cross sections are presently available only for ¹²C and ⁵⁶Fe target nuclei, obtained by the LSND [1] and KARMEN [2, 3] collaborations, and at LAMPF [4]. At present only theoretical approaches can provide cross sections for a large number of target nuclei that are involved in various applications of neutrino physics and astrophysics. It is, therefore, crucial to quantitatively assess the theoretical uncertainties in modeling neutrino induced processes, including the detailed structure of principal transitions involved, and the total cross sections averaged over selected neutrino fluxes. The evaluation of current theoretical uncertainties in modeling neutrino induced processes is also important in view of future experimental programs, e.g., spallation neutron source (SNS) at ORNL [5], Large Volume Detector in Gran Sasso (LVD) [6], and the beta-beams for the production of neutrinos by using the β -decay of boosted radioactive ions [7, 8].

Over the years a variety of microscopic models have been developed and employed in the calculation of neutrino-nucleus cross sections at low energies. These include the shell model [9–13], the random phase approximation (RPA) [12, 14, 15], continuum RPA (CRPA) [16–18], hybrid models of CRPA and shell model [14, 19], Fermi gas model [20], quasiparticle RPA [21, 22], projected QRPA [23], and relativistic quasiparticle RPA (RQRPA) [24]. For the purpose of the present analysis of theoretical uncertainties in modeling neutrino-nucleus cross sections, we chose the iron group nuclei for which the framework based on the energy density functionals and the shell model represent feasible approaches and, in addition, data from muon decay at rest (DAR) are available [2, 3]. The framework based on energy density functionals employs the Relativistic Hartree-Bogoliubov

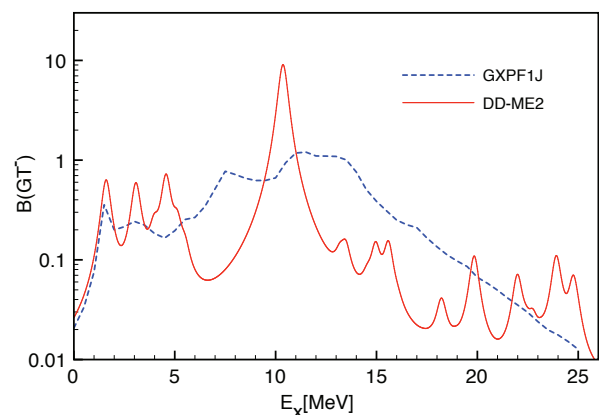


FIG. 1. (Color online) GT^- transition strength in ⁵⁶Fe, calculated using the RQRPA (DD-ME2) and the Shell model (GXPf1J).

model (RHB) to determine the nuclear ground state, and the RQRPA to calculate all relevant transitions induced by the incoming neutrinos [24]. Model calculations are performed using effective interactions with density-dependent meson-nucleon couplings, in this case the DD-ME2 interaction [25], whereas pairing correlations are described by the finite range Gogny force [26]. The nuclear shell model employed in the present study is based on the GXPf1J effective interaction [27] for $\lambda^\pi = 1^+$ channel, supplemented by the RPA based on a Skyrme functional (SGII) for other multipoles [13]. A detailed analysis of (anti)neutrino - ⁵⁶Fe cross sections based on the QRPA with Skyrme functionals is given in Ref. [21]. Shell-model calculations are carried out with the code MSHELL [28].

Because of its importance for neutrino-nucleus cross sections at low energies, we start by analyzing the Gamow-Teller(GT) transition strength in the iron group

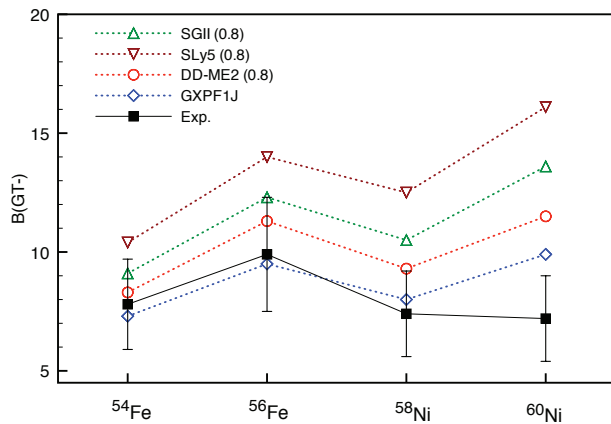


FIG. 2. (Color online) GT^- transition strengths calculated with the Skyrme RPA (SGII, SLy5) and RQRPA (DD-ME2), in comparison to the shell model (GXPF1J) [13] and experimental values [29]. (Q)RPA calculations include the quenching factor 0.8 in the axial-vector coupling constant g_A .

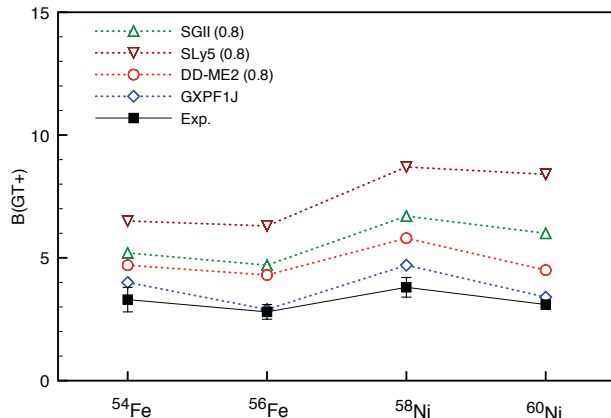


FIG. 3. (Color online) Same as described in the caption to Fig.2 but for the GT^+ transitions. Experimental values are from Refs. [30–32].

nuclei. Fig. 1 displays the GT^- strength distributions for ^{56}Fe , obtained using the shell model (GXPF1J) and the RQRPA (DD-ME2). In both cases the calculated transition strength is folded by a Lorentzian with the width $\Gamma=0.5$ MeV. The RQRPA includes only $2qp$ configurations and, therefore, cannot provide the detailed structure of excitation spectra obtained by the shell model. Nevertheless, one can observe that the calculated transition strength distributions are in reasonable agreement.

In Figs. 2 and 3 the GT^\pm transition strengths contributing to the neutrino-induced processes are compared for a set of iron group nuclei: $^{54,56}\text{Fe}$ and $^{58,60}\text{Ni}$. The following models and respective parameterizations have been used: i) RPA based on Skyrme functionals (SGII, SLy5), ii) RQRPA (DD-ME2) [25], and iii) shell model (GXPF1J) [13]. Results of model calculations are

TABLE I. GT^- transition strengths calculated using the Skyrme RPA (SGII, SLy5), RQRPA (DD-ME2), and shell model (GXPF1J) [13] (all using $g_A^* = 0.74g_A$), compared to experimental values [29].

	⁵⁴ Fe	⁵⁶ Fe	⁵⁸ Ni	⁶⁰ Ni
SGII	7.8	10.5	9.0	11.7
SLy5	8.9	11.9	10.7	13.8
DD-ME2	7.1	9.7	7.9	9.8
GXPF1J	7.3	9.5	8.0	9.9
Exp.	7.8 ± 1.9	9.9 ± 2.4	7.4 ± 1.8	7.2 ± 1.8

compared with the data for GT^- [29] and GT^+ [30–32] transition strengths. The (Q)RPA calculations include the quenching of the free-nucleon axial-vector coupling constant $g_A = 1.262 \rightarrow g_A = 1$, corresponding to the quenching factor 0.8 in the GT transition operator. A quenching factor is also used in the shell model. However, its value 0.74 is adapted to the effective interaction and model space under consideration [13]. One notices in Figs. 2 and 3 that the shell model reproduces the experimental values of GT^- transition strength with high accuracy (except for ^{60}Ni), and also the GT^+ strength is reasonably reproduced. (Q)RPA based approaches, however, even by quenching the value $g_A \rightarrow 1$, overestimate both the GT^- and GT^+ transition strengths. For $^{54,56}\text{Fe}$ and ^{58}Ni the relativistic QRPA results for the $B(GT^-)$ are within experimental uncertainties. The fact that QRPA calculations systematically overestimate the measured GT^\pm transition strength, even though different effective interactions are used, indicates that a somewhat stronger quenching of the axial-vector coupling constant might be necessary to reproduce the data. Actually, if the same quenching factor 0.74 used by the shell model is also employed in (Q)RPA calculations, a very good agreement with the shell-model results is obtained. The (Q)RPA and shell model $B(GT^-)$ values, all obtained using the same quenching factor 0.74, are shown in Table I in comparison to the data [29]. In this case for all four nuclei: $^{54,56}\text{Fe}$ and $^{58,60}\text{Ni}$, the (Q)RPA $B(GT^-)$ values are found in good agreement with the shell-model results, particularly for the relativistic QRPA (DD-ME2). We have verified that the same result is also obtained for the $B(GT^+)$ channel. This similarity is not obvious as the two theoretical frameworks have different foundations, use different effective interactions and model spaces, that is, the underlying structure cannot be directly compared, except for the resulting observables that one confronts to data. This result should also be considered with caution because of well known problem of missing GT strength, due either to excitations that involve complex configurations at higher excitation energies, or excitations that include non-nucleonic degrees of freedom.

As already emphasized in previous studies of neutrino-nucleus reactions [21, 24], not only GT^- transitions but

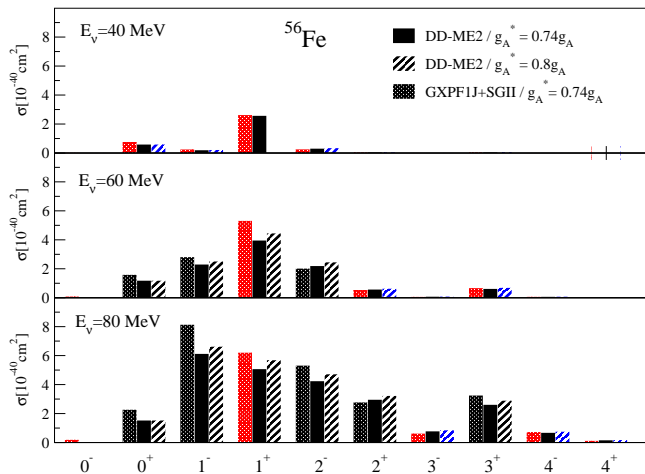


FIG. 4. (Color online) Contributions of the multipole transitions $\lambda^\pi = 0^\pm - 4^\pm$ to the inclusive cross section for the $^{56}\text{Fe}(\nu_e, e^-)^{56}\text{Co}$ reaction, at $E_{\nu_e} = 40, 60$ and 80 MeV. Calculations include RHB+RQRPA (DD-ME2), and the shell model (GXPF1J) (for the 1^+ transition) plus the RPA (SGII) for higher multipoles. The quenching factors in g_A are denoted in the figure.

also excitations of higher multipoles must be included, depending on the energy range under consideration. In this work we analyze the reaction $^{56}\text{Fe}(\nu_e, e^-)^{56}\text{Co}$ in more detail, using two representative theoretical approaches: the shell model (GXPF1J) supplemented by the RPA based on Skyrme functionals (SGII), and the fully consistent relativistic framework RHB+QRPA (DD-ME2). The goal is to provide an estimate of theoretical uncertainties of contributions from different multipole transitions to the neutrino cross section. In Fig. 4 we plot the contributions of the multipole transitions $\lambda^\pi = 0^\pm - 4^\pm$ to the inclusive cross section for the $^{56}\text{Fe}(\nu_e, e^-)^{56}\text{Co}$ reaction, at $E_{\nu_e} = 40, 60$ and 80 MeV. The RHB+RQRPA (DD-ME2) calculations include the standard (0.8), and enhanced (0.74) quenching factors of the axial-vector coupling constant g_A in all multipole operators. In the non-relativistic framework the shell model (GXPF1J) is used for 1^+ transitions, and RPA (SGII) is used for higher multipoles. The quenching factor for the axial-vector coupling g_A is 0.74. In the shell model calculation of 1^+ transitions the effect of finite momentum transfer (q) is taken into account by evaluating the matrix elements $\langle f || j_0(qR) [Y^0 \times \vec{\sigma}]^1 t_- || i \rangle$ and $\langle f || j_2(qR) [Y^2 \times \vec{\sigma}]^1 t_- || i \rangle$ at each q , instead of the approximate treatment of Ref. [13] where the GT matrix element $\langle f || j_0(qR) \vec{\sigma} t_- || i \rangle$ was evaluated multiplied by $j_0(qR)$ (R is the nuclear radius).

At relatively low neutrino energies ($E_\nu \lesssim 40$ MeV) the dominant contribution to the calculated cross sections originates from GT transitions ($\lambda^\pi = 1^+$). With increasing E_ν , however, contributions from other multipole transitions become important. In particular, at $E_\nu = 80$ MeV the dominant transition is the spin-dipole $\lambda^\pi = 1^-$,

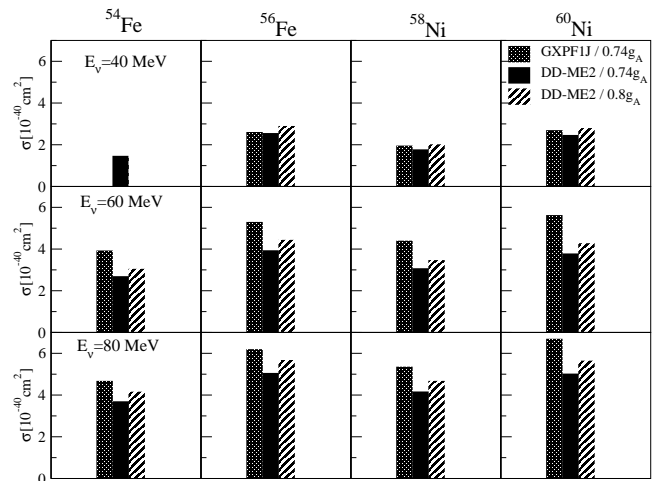


FIG. 5. (Color online) Inclusive neutrino-nucleus cross sections in the 1^+ channel for the $^{54,56}\text{Fe}$ and $^{58,60}\text{Ni}$ target nuclei, at the incoming neutrino energies $E_{\nu_e} = 40, 60$ and 80 MeV. The results are obtained using the RHB+RQRPA (DD-ME2) framework, and the shell model (GXPF1J). The axial-vector coupling g_A^* includes a quenching factor as denoted in the figure.

but also other components, e.g. $\lambda^\pi = 1^+, 2^-, 2^+, 3^+$, play an important role. The cross sections plotted in Fig. 4 show that the two models predict a very similar structure and distribution of the relative contributions from various multipoles. These results are also in agreement with those discussed in Ref. [21].

In Fig. 5 we compare the neutrino-capture cross sections for the $\lambda^\pi = 1^+$ channel on the set of target nuclei: $^{54,56}\text{Fe}$ and $^{58,60}\text{Ni}$, and for the incoming neutrino energies $E_{\nu_e} = 40, 60$ and 80 MeV. The results are obtained using the RHB+RQRPA (DD-ME2) and the shell model (GXPF1J). The axial-vector coupling g_A^* includes a quenching factor as denoted in the figure. The cross sections increase in heavier isotopes because electron neutrinos are captured on neutrons. The two models, although based on different microscopic pictures, predict rather similar cross sections. One notes that at higher neutrino energies the shell model cross sections are slightly larger than those calculated with the RQRPA. Related to the previous discussion on the overall GT strength and the quenching of g_A , from the cross sections shown in Fig. 5 it appears that the (Q)RPA does not require a stronger quenching than the usual $g_A = 1$ to be in agreement with the shell model. The reason is that the calculated cross sections are not only determined by the overall GT transition strength, but also by the transition energies that govern the energies of outgoing electrons.

We have also analyzed cross sections averaged over the neutrino flux described by the Fermi-Dirac spectrum [24]. Figure 6 displays the flux-averaged cross sections for the reaction $^{56}\text{Fe}(\nu_e, e^-)^{56}\text{Co}$, evaluated at different temperatures in the interval $T = 2 - 10$ MeV, and for the chemical potential $\alpha = 0$. The RHB+RQRPA (DD-ME2)

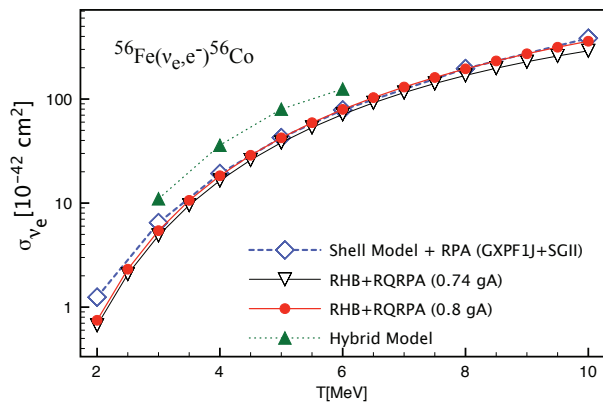


FIG. 6. (Color online) Neutrino - ^{56}Fe cross sections averaged over the Fermi-Dirac distribution. The RHB+RQRPA (DD-ME2) calculations including the standard (0.8), and enhanced (0.74) quenching factors of the axial-vector coupling g_A , are compared to shell model + RPA results [13], and those obtained using a hybrid model of Ref. [33].

calculations including the standard (0.8), and enhanced (0.74) quenching factors in g_A , are compared to the shell model + RPA (GXPF1J + SGII) results [13], and those obtained using a hybrid model of Ref. [33]. The latter model predicts somewhat larger cross sections, whereas a very good agreement is found between the results of shell model + RPA and RQRPA.

The theoretical cross sections for the reaction $^{56}\text{Fe}(\nu_e, e^-)^{56}\text{Co}$ can also be analyzed in comparison to data from the KARMEN collaboration. The calculated cross sections are averaged over the neutrino flux described by the Michel spectrum obtained from muon decay-at-rest (DAR): $f(E_{\nu_e}) = (96E_{\nu_e}^2/m_\mu^4)(m_\mu - 2E_{\nu_e})$. Taking into account the results obtained in this work with the RHB+RQRPA (DD-ME2) - $263 \times 10^{-42}\text{cm}^2$, shell model (GXPF1J) (for 1^+ transitions) plus the RPA (SGII) for other multipoles - $259 \times 10^{-42}\text{cm}^2$, as well as results from previous studies that used the RPA with a Landau-Migdal force - $240 \times 10^{-42}\text{cm}^2$ [33], the QRPA(SIII) - $352 \times$

10^{-42}cm^2 [21] and the QRPA based on G-matrix formalism - $173.5 \times 10^{-42}\text{cm}^2$ [22], the DAR neutrino-nucleus cross section and its theoretical uncertainty are estimated to be: $\langle \sigma \rangle_{th} = (258 \pm 57) \times 10^{-42}\text{cm}^2$. This value is in very good agreement with the data from the KARMEN collaboration: $\langle \sigma \rangle_{exp} = (256 \pm 108 \pm 43) \times 10^{-42}\text{cm}^2$. We note that the various models used to obtain the theoretical estimate employ different effective interactions, and also comprise a wide range of values for the axial-vector coupling, from those without quenching [21, 22] to models that use a quenching factor of 0.7 [33]. All theory frameworks, except the QRPA based on G-matrix formalism, favor the quenching of the axial-vector coupling constant g_A , in accordance to constraints given by the experimental data on Gamow-Teller transitions. The implementation of the quenching of g_A in QRPA based on Skyrme functionals [21] would lower the calculated neutrino-nucleus cross sections and it would further reduce the overall theoretical uncertainty in $\langle \sigma \rangle_{th}$.

In conclusion, the charged current neutrino-nucleus cross sections for $^{54,56}\text{Fe}$ and $^{58,60}\text{Ni}$ have been analyzed by employing models based on the relativistic and Skyrme energy density functionals, and the shell model. The theoretical uncertainties in modeling neutrino induced processes have been examined by considering the Gamow-Teller transition strength and available data, the multipole decomposition of the calculated cross sections, and cross sections averaged over the Michel flux and Fermi-Dirac distribution. It has been shown that various models predict very similar multipole distributions of neutrino-nucleus cross sections. The corresponding cross sections averaged over the DAR neutrino spectra show that the current theoretical uncertainty, despite a variety of models and effective interactions that have been used in many studies, is actually smaller than the experimental one, and could be even further reduced by constraining the quenching of the axial-vector coupling constant g_A to data for the Gamow-Teller transition strength.

ACKNOWLEDGMENTS

This work is supported by MZOS - project 1191005-1010, the Croatian Science Foundation, and Grants-in-Aid for Scientific Research (C) 22540290 of the MEXT of Japan.

-
- [1] C. Athanassopoulos et al., Phys. Rev. C 55, 2078 (1997).
 - [2] B. E. Bodmann et al., Phys. Lett. B 332, 251 (1994).
 - [3] R. Maschuw, Prog. Part. Nucl. Phys. 40, 183 (1998).
 - [4] D. A. Krakauer et al., Phys. Rev. C 45, 2450 (1992).
 - [5] F. T. Avignone, L. Chatterjee, Yu. V. Efremenko, M. Strayer, J. Phys. G 29, 2497 (2003).
 - [6] N.Yu. Agafonova et al., Astron. Phys. 27, 254 (2007).
 - [7] P. Zucchelli, Phys. Lett. B 532, 166 (2002).
 - [8] C. Volpe, J. Phys. G 30, L1 (2004).
 - [9] W. C. Haxton, Phys. Rev. D 36, 2283 (1987).
 - [10] J. Engel, E. Kolbe, K. Langanke, and P. Vogel, Phys. Rev. C 54, 2740 (1996).
 - [11] A. C. Hayes and I. S. Towner, Phys. Rev. C 61, 044603 (2000).
 - [12] C. Volpe, N. Auerbach, G. Colò, T. Suzuki, and N. Van Giai, Phys. Rev. C 62, 015501 (2000).
 - [13] T. Suzuki, M. Honma, K. Higashiyama, T. Yoshida, T. Kajino, T. Otsuka, H. Umeda, and K. Nomoto, Phys. Rev. C 79, 061603(R) (2009).
 - [14] N. Auerbach, N. Van Giai, and O. K. Vorov, Phys. Rev. C 56, R2368 (1997).
 - [15] S. K. Singh, N. C. Mukhopadhyay, and E. Oset, Phys. Rev. C 57, 2687 (1998).
 - [16] E. Kolbe, K. Langanke, S. Krewald, F.-K. Thielemann,

- Nucl. Phys. A 540, 599 (1992).
- [17] N. Jachowicz, S. Rombouts, K. Heyde, and J. Ryckebusch, Phys. Rev. C 59, 3246 (1999).
- [18] A. Botrugno and G. Co', Nucl. Phys. A 761, 200 (2005).
- [19] E. Kolbe, K. Langanke, and G. Martínez-Pinedo, Phys. Rev. C 60, 052801 (1999).
- [20] T. Kuramoto, M. Fukugita, Y. Kohyama, and K. Kubodera, Nucl. Phys. A 512, 711 (1990).
- [21] R. Lazauskas and C. Volpe, Nucl. Phys. A 792, 219 (2007).
- [22] M. K. Cheoun, E. Ha, K. S. Kim, and T. Kajino, J. Phys. G 37, 055101 (2010).
- [23] A. R. Samana, F. Krmpotic, N. Paar, and C. A. Bertulani, Phys. Rev. C 83, 045807 (2011).
- [24] N. Paar, D. Vretenar, T. Marketin, and P. Ring, Phys. Rev. C 77, 024608 (2008).
- [25] G. A. Lalazissis, T. Nikšić, D. Vretenar, and P. Ring, Phys. Rev. C 71, 024312 (2005).
- [26] J. F. Berger, M. Girod, and D. Gogny, Comp. Phys. Comm. 63, 365 (1991).
- [27] M. Honma, T. Otsuka, T. Mizusaki, M. Hjorth-Jensen and B. A. Brown, J. of Phys.: Conf. Series 20, 7 (2005).
- [28] T. Mizusaki, RIKEN Accel. Prog. Rep. 33, 14 (2000).
- [29] J. Rapaport et al., Nucl. Phys. A 410, 371 (1983).
- [30] M. C. Wetterli et al., Phys. Rev. C 40, 559 (1989).
- [31] S. El-Kateb et al., Phys. Rev. C 49, 3128 (1994).
- [32] A. L. Williams et al., Phys. Rev. C 51, 1144 (1995).
- [33] E. Kolbe and K. Langanke, Phys. Rev. C 63, 025802 (2001).